

Ubiquity of shallow mesoscale circulations in the trades and their influence on moisture variance

Geet George¹, Bjorn Stevens¹, Sandrine Bony², Raphaela Vogel², and Ann Kristin Naumann¹

¹Max Planck Institute for Meteorology, Hamburg, Germany

²LMD/IPSL, Sorbonne University, CNRS, Paris, France

September 19, 2022

Abstract

Understanding drivers of cloud organization is crucial for accurately estimating clouds' feedback to a warming climate. Shallow mesoscale circulations are thought to play an important role in cloud organization, but they have not been observed. Here, we present observational evidence for shallow mesoscale overturning circulations (SMOCs) from divergence measurements made during the EUREC4A field campaign in the north-Atlantic trades. Meteorological reanalyses reproduce the observed low-level divergence well and confirm SMOCs to be mesoscale features (ca. 200 km). Large mesoscale variability, five-fold the mean, is shown to be associated with the ubiquity of SMOCs. Furthermore, time-lag correlations suggest that SMOCs amplify mesoscale moisture variance at cloud-base and in the sub-cloud layer. Through their modulation of cloud-base moisture, SMOCs influence the drying efficiency of entrainment, thus yielding moist ascending branches and dry descending branches. The observed moisture variance differs from expectations from large-eddy simulations, which show largest variance near cloud top and negligible sub-cloud variance. The ubiquity of SMOCs and their coupling to moisture and cloud fields suggest that the strength and scale of mesoscale circulations are important in determining how clouds couple to climate, something which is not considered by present theories.

1 Ubiquity of shallow mesoscale circulations in the trades and their
2 influence on moisture variance

3 Geet George^{1,*}, Bjorn Stevens¹, Sandrine Bony², Raphaela Vogel^{2,3}, and Ann Kristin
4 Naumann^{1,3}

5 ¹Max Planck Institute for Meteorology, Hamburg, Germany

6 ²LMD/IPSL, Sorbonne University, CNRS, Paris, France

7 ³Meteorological Institute, Universität Hamburg, Hamburg, Germany

8 *Corresponding author: Geet George, geet.george@mpimet.mpg.de

9 September 4, 2022

Abstract

Understanding drivers of cloud organization is crucial for accurately estimating clouds' feedback to a warming climate. Shallow mesoscale circulations are thought to play an important role in cloud organization, but they have not been observed. Here, we present observational evidence for shallow mesoscale overturning circulations (SMOCs) from divergence measurements made during the EUREC⁴A field campaign in the north-Atlantic trades. Meteorological reanalyses reproduce the observed low-level divergence well and confirm SMOCs to be mesoscale features (ca. 200 km). Large mesoscale variability, five-fold the mean, is shown to be associated with the ubiquity of SMOCs. Furthermore, time-lag correlations suggest that SMOCs amplify mesoscale moisture variance at cloud-base and in the sub-cloud layer. Through their modulation of cloud-base moisture, SMOCs influence the drying efficiency of entrainment, thus yielding moist ascending branches and dry descending branches. The observed moisture variance differs from expectations from large-eddy simulations, which show largest variance near cloud top and negligible sub-cloud variance. The ubiquity of SMOCs and their coupling to moisture and cloud fields suggest that the strength and scale of mesoscale circulations are important in determining how clouds couple to climate, something which is not considered by present theories.

27 An understanding of the coupling between clouds and atmospheric circulation – one of the
 28 World Climate Research Programme’s seven Grand Challenges – is a crucial missing link for
 29 constraining estimates of cloud feedback, i.e. the response of clouds to a warming climate [1,
 30 2]. Cloud feedback estimates, especially those associated with low clouds, constitute one of
 31 the largest uncertainties in current assessments of climate sensitivity [3, 4]. The link between
 32 circulation and moisture variance at mesoscales ($\mathcal{O}(100 \text{ km}, 1 \text{ h})$) influences the amount of clouds
 33 [5, 6] as well as their spatial organization [7]. Both aspects are crucial for low-cloud feedback [6,
 34 8, 9]. Idealized large domain large-eddy simulations (LES) show that the spatial organization
 35 of clouds is coupled to shallow overturning circulations, which create moist and dry anomalies
 36 in their ascending and descending branches, respectively [10, 11, 12]. These circulations, while
 37 present in LES, are absent in the conceptual frameworks used to represent clouds in global
 38 climate models. This increases interest in determining if such circulations are evident in nature,
 39 and if so just how prevalent they are.

40 Recently, the field campaign EUREC⁴A [*Elucidating the RolE of Cloud-Circulation Cou-*
 41 *pling in ClimAte*; 13, 14] made extensive measurements of mesoscale horizontal divergence (\mathcal{D}),
 42 making it possible to explore the presence of such circulations and thus test inferences from
 43 modelling. The \mathcal{D} measurements are samples averaged over a $\sim 220 \text{ km}$ diameter circle for $\sim 1 \text{ h}$
 44 in the north-Atlantic trades [14, 15, 16], hereforth referred to as *circles* (Fig 1a,d). We analyze
 45 65 circles from 11 flights spread over four weeks in January-February 2020. As shown in Fig. 1,
 46 a *flight-day* typically included two *circling-sets* (three consecutive circles) separated by an hour.
 47 Using EUREC⁴A measurements we: (a) present observational evidence for shallow mesoscale
 48 overturning circulations (SMOCs hereafter), (b) characterize their spatial scales and frequency
 49 of occurrence with help from meteorological reanalysis and (c) propose a mechanism by which
 50 SMOCs amplify moisture variance.

51 Evidence of SMOCs in EUREC⁴A measurements

52 The time-mean \mathcal{D} (Fig. 1b) is consistent with the theoretical understanding of the trades be-
 53 ing on average a region of weak subsidence (ω) [17]. In the free troposphere, time-mean ω
 54 ($\sim 24 \text{ hPa day}^{-1}$) as per the weak temperature gradient [WTG; 18] assumption, balances a
 55 mean cooling of $\sim 1.3 \text{ K day}^{-1}$, consistent with observed climatological cooling in the trades [19,
 56 20]. \mathcal{D} increases from the surface upwards and is then roughly constant through the bulk of the

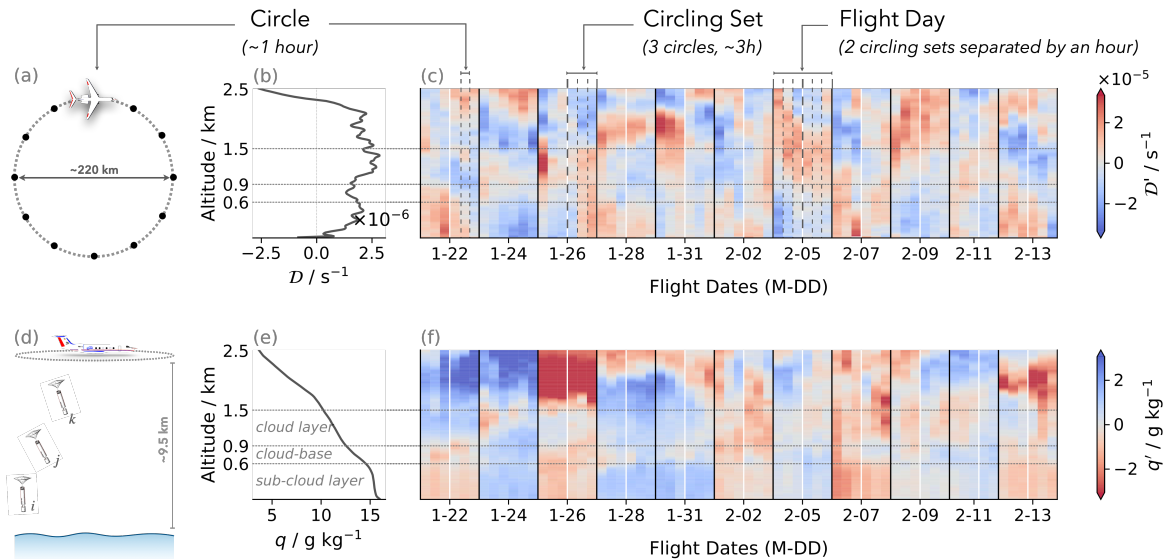


Figure 1: Divergence and humidity measurements from EUREC^{4A} | Vertical profiles of (b) divergence \mathcal{D} and (e) specific humidity q averaged over EUREC^{4A} circles. Anomalies of \mathcal{D} and q from time-mean (\mathcal{D}' and q') are shown as hues in (c) and (f), respectively. Descriptions of terms explaining the sampling strategy (*circle*, *circling set* and *flight day*) are for typical samples. Deviations in some cases are detailed in [5] and [15]. The schematic on the left shows: (a) top-view of the HALO aircraft flying a circle with markers representing launch location of dropsondes and (d) a side-view depiction of multiple dropsondes (i, j, k) in flight.

57 trade-wind layer (0.3 - 2.3 km). This vertical coherence, however, is restricted to the time-mean
 58 and thus representative only of the larger synoptic scale.

59 At shorter timescales, \mathcal{D} departs markedly from time-mean (Fig. 1c) indicating large vertical
 60 velocities unbalanced by radiation. The divergence anomaly (\mathcal{D}') also changes sign between the
 61 sub-cloud and cloud layers. Averaged over circling-set and flight-day means (~ 3 and $\sim 6-7$ h,
 62 respectively), we find an anti-correlation between \mathcal{D}' averaged over the sub-cloud (\mathcal{D}'_{sc}) and
 63 cloud layer (\mathcal{D}'_c) (Fig. 2a). Thus, when there is convergence in the sub-cloud layer, air diverges
 64 in the cloud layer and vice-versa. The prevalence of this \mathcal{D}' dipole in the lower atmosphere
 65 indicates the presence of shallow overturning circulations, with circles sampling either ascending
 66 or descending branches. Given EUREC^{4A}'s unbiased sampling and the sign changes in \mathcal{D} over
 67 consecutive flights, we believe that the dipole is a mesoscale feature that is almost always
 68 apparent.

69 We investigate the vertical structure of these circulations, by analyzing composites of the
 70 lowest and highest quartiles of \mathcal{D}_{sc} (Figs. 3a-d). To distinguish the circulation features, analyses
 71 in Fig. 3 excludes data from 24.01.2020, the only day with flight-day mean missing the \mathcal{D}'
 72 dipole (data-point in lower-left quadrant in Fig. 2a). Figs. 3a,b suggest that the circulations
 73 are shallow, being largely confined to the trade-wind layer (lower ~ 2.3 km). The shallowness

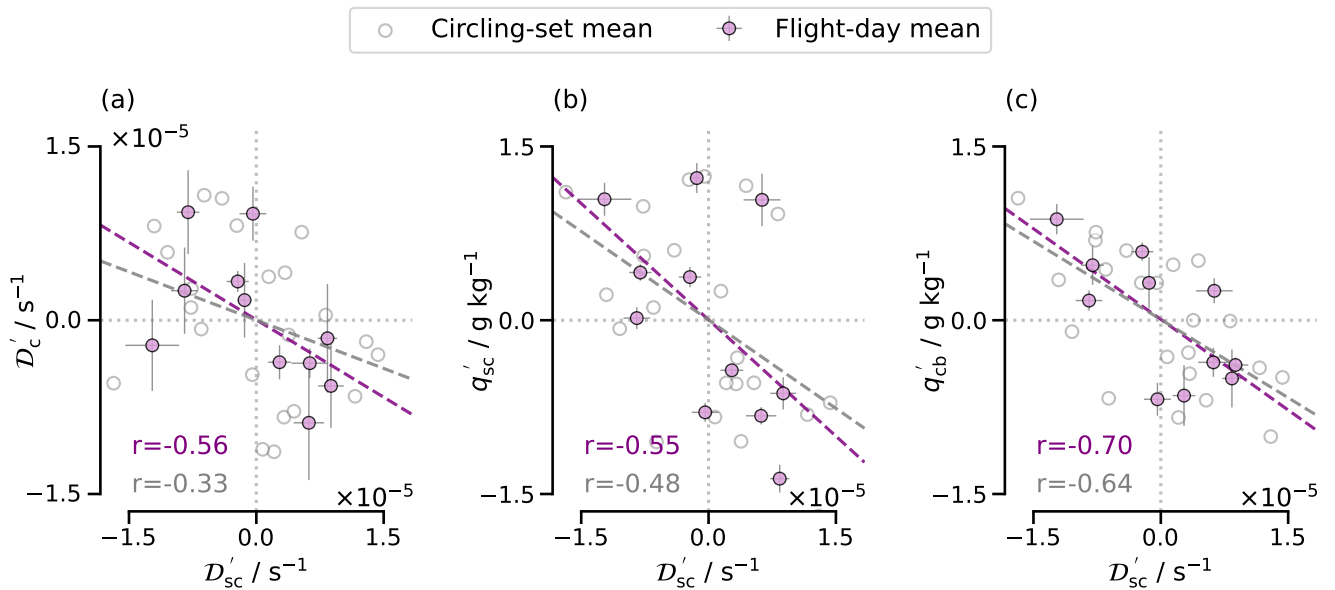


Figure 2: Relationships with sub-cloud layer divergence | Scatter plots against D'_{sc} of (a) D'_c , (b) q'_{sc} and (c) q'_{cb} . Subscripts ‘sc’, ‘cb’ and ‘c’ stand for averaging over sub-cloud (0-600 m), cloud-base (600-900 m) and cloud (900-1500 m) layers, respectively. Cross hairs show the standard deviation in the mean along altitude. r -values indicate Pearson’s correlation coefficient for flight-day means (pink) and circling-set means (purple).

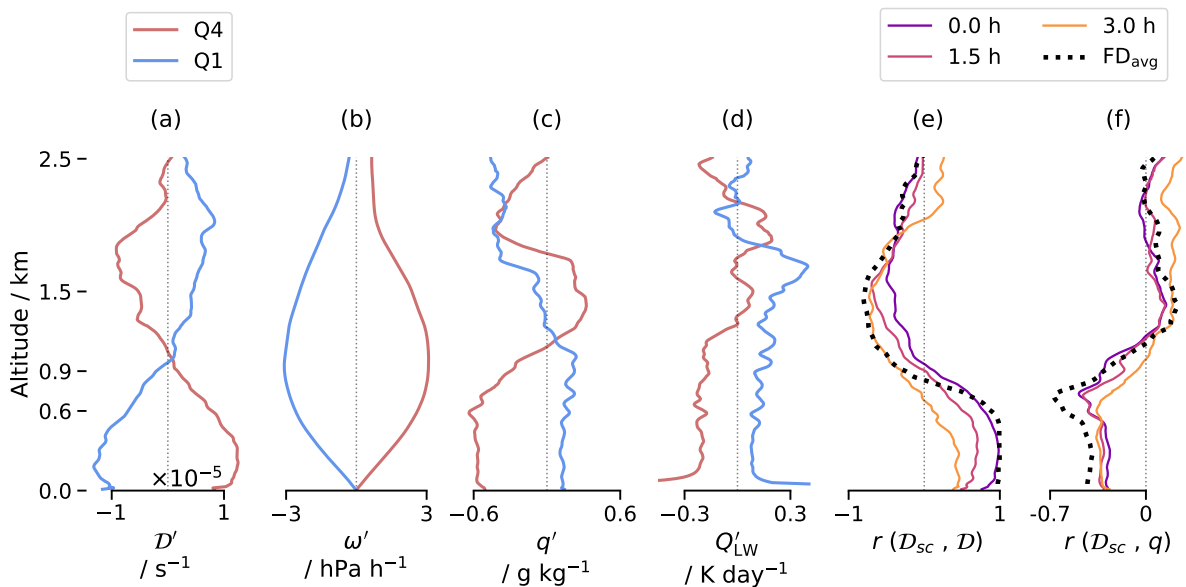


Figure 3: Quartile composites and correlations with sub-cloud divergence | Averaged profiles of anomalies of (a) D (b) subsidence ω , (c) q and (d) net longwave radiative cooling rate Q'_{LW} are shown for the lowest (Q1; strongest convergence) and highest (Q4; strongest divergence) quartiles of D_{sc} . Vertical profiles of Pearson’s correlation coefficients (r -value) are shown between (e) D_{sc} and D and (f) D_{sc} and q . Dashed lines show correlation from flight-day averages (FD_{avg}), whereas the coloured profiles show correlation from circle-scale, but D lagging D_{sc} in time as indicated in the legend. Profiles exclude circles from flight on 24.01.2020.

74 is made further evident by the fact that the strongest anti-correlation of \mathcal{D} with \mathcal{D}_{sc} happens
 75 within and throughout the cloud layer (Fig. 3e). This shallowness is not unexpected given the
 76 large values of \mathcal{D}' (Fig. 3a), which if maintained over a deeper layer would imply much larger
 77 ω' . Even for circulations as shallow as those observed, ω' goes up to 3 hPa hr^{-1} (Fig. 3b),
 78 which if sustained over a period of a day, would imply displacements of $\sim 670 \text{ m day}^{-1}$. If not
 79 compensated by adjacent branches of similar magnitude, such large displacements would lead
 80 to large pressure gradients and a deep saturated layer in the ascending branch, both of which
 81 are inconsistent with the shallow convective nature of the wintertime trades.

82 Ubiquity and spatial scale of SMOCs

83 To further test the idea that the circulations are mesoscale, we look into the European Centre
 84 for Medium-Range Weather Forecasts (ECMWF) reanalysis product [ERA5; 21] over a $10^\circ \times$
 85 10° domain, available at 0.25° spatial and 1 h temporal intervals. Reanalyses are thought to
 86 be reliable only for their synoptic reconstruction of divergence [e.g. 22, 23]. However, ERA5
 87 turns out to reproduce mesoscale \mathcal{D} from the EUREC⁴A measurements in the lowest $\sim 2.5 \text{ km}$
 88 (see Fig. ED.1), and it does so independent of the assimilation of EUREC⁴A soundings (see
 89 Methods). This ability of ERA5 to reproduce mesoscale \mathcal{D} is likely due to the assimilation of
 90 scatterometer winds at the ocean surface and therefore presumably not limited to the EUREC⁴A
 91 region and period.

92 ERA5's ability to capture \mathcal{D} allows us to investigate SMOCs' occurrence and spatial coverage.
 93 Similar to the measurements, we identify SMOCs in ERA5, by selecting grid points with a \mathcal{D}'
 94 dipole. We then cluster such grid points into SMOC objects and fit them to equivalent ellipses
 95 (see Methods and Figs. 4a,b) to quantify their shape, size and orientation. Strikingly, SMOCs
 96 are present over the entire domain in Fig. 4a,b. We see a similar spatial prevalence of SMOCs for
 97 the entire EUREC⁴A period: $58 \pm 7\%$ of the domain is covered by SMOCs (also see Fig. ED.3).
 98 The prevalence of the \mathcal{D}' dipole in circles, combined with the spatio-temporal omnipresence of
 99 SMOCs in ERA5 shows that SMOCs are ubiquitous in the downstream trades.

100 Fig. 4c shows the distribution of the major and minor axes lengths and effective diameters
 101 (d_{eff}) of SMOC objects for the EUREC⁴A period. The median values of all three lengths lie
 102 between 80 and 200 km, quantifying the size of these circulations' branches. This spatial scale
 103 derived from ERA5 fits well with the scale estimated from the measurements. The correlation of

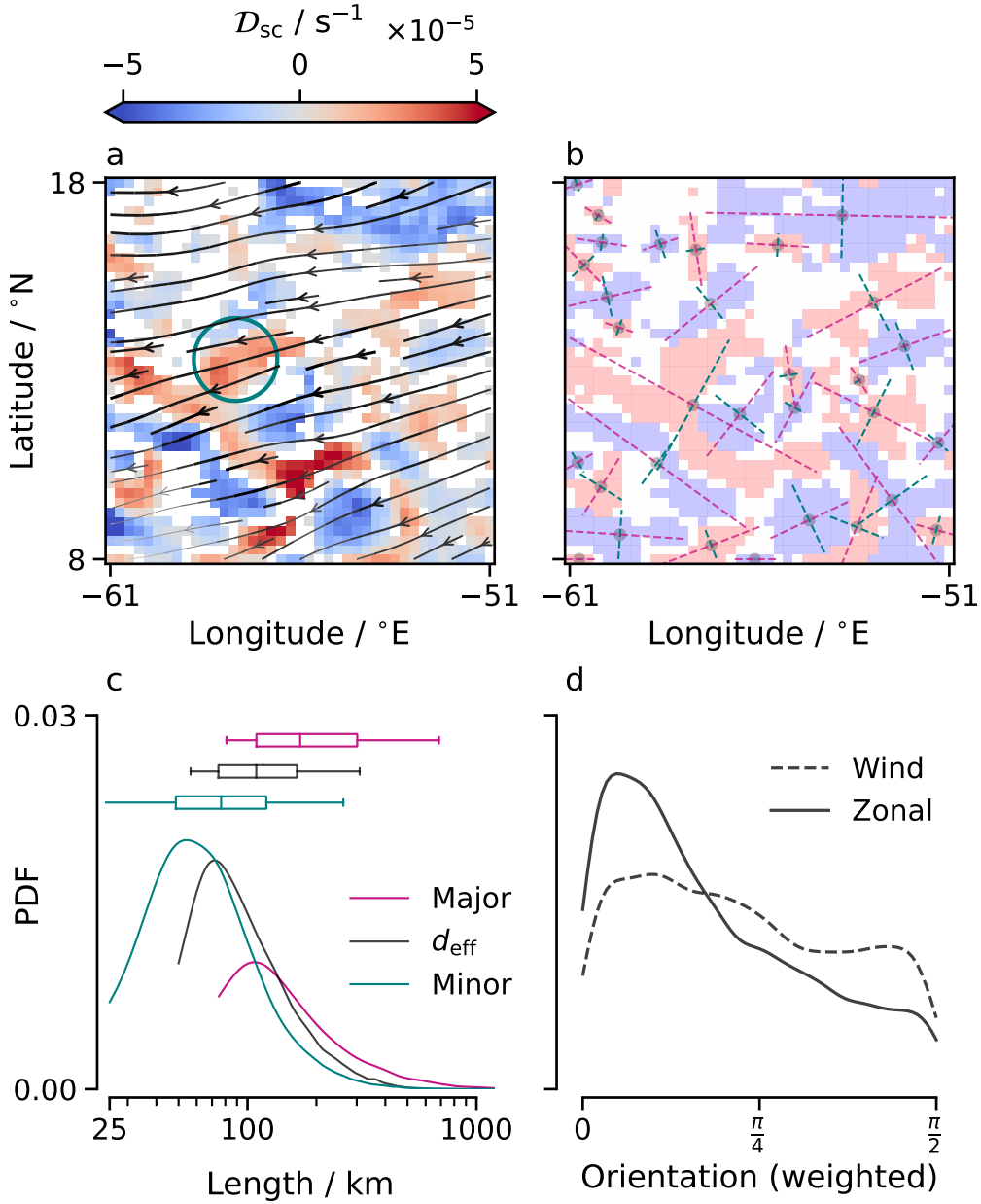


Figure 4: Scale and orientation of SMOC objects in reanalyses | (a) and (b) show a typical snapshot of ERA5 D'_{sc} for a $10^\circ \times 10^\circ$ domain (2020-02-14 09:00 UTC). Overlaid streamlines in (a) show horizontal wind in the sub-cloud layer; thicker lines indicate stronger winds. The circle (teal) indicates the EUREC⁴A circle. Similar D'_{sc} maps at 12 h snapshots for January-February, 2020 are shown in Fig. ED.3. Shading in (b) indicates convergent (blue) and divergent (red) clusters, with the centroid, major axis and minor axis, are shown for the SMOC objects (see Methods for details). (c) Gaussian-kernel probability density function (PDF; bin width ~ 2 km) of major axis length (orange), minor axis length (green) and effective diameter (d_{eff} ; black) for all SMOCs objects detected in the same domain every hour during the EUREC⁴A period. Box-plots above show median (line in box), first and third quartiles (ends of box) and 5th and 95th percentiles (ends of whiskers). Lengths (in km) are derived with the approximation that $1^\circ \simeq 100$ km. (d) PDF (bin width $\pi/150$) of orientation of SMOC objects weighted by their area, with 0 indicating parallel and $\pi/2$ indicating tangential alignment of the major axis.

104 \mathcal{D} with \mathcal{D}_{sc} (Fig. 3e) shows that SMOCs persist for longer than 1 h, as the peak anti-correlation
 105 between \mathcal{D}_c and \mathcal{D}_{sc} occurs 2-3 hours apart, with \mathcal{D}_c lagging \mathcal{D}_{sc} . Considering 9 m s^{-1} winds,
 106 airmasses would traverse the circle in ~ 7 h (see Fig. 5) and flight-day measurements spanned
 107 ~ 8 h. Hence, if SMOCs are of similar spatial scales as in Fig. 4c, one flight would sample only
 108 one branch of the circulation, which is consistent with what we observe, as \mathcal{D}'_{sc} rarely changes
 109 signs through the course of a flight-day (Fig. 1c). These spatial scales, along with the adjacency
 110 of convergent and divergent cells, confirm that the dipole signals in measurements are indeed
 111 from circulations at the mesoscale.

112 Most SMOC objects are elongated rather than circular, as indicated by the offset between
 113 the major and minor axes length distributions in Fig. 4c. Fig. 4d shows that the elongation
 114 tends to align in the zonal direction, but there is little indication that SMOCs are concentrated
 115 along the direction of the near-surface (or cloud base) zonal wind.

116 Moisture variance and maintenance of SMOCs

117 SMOCs covary with the mesoscale moisture fields. Figs. 2b,c show that sub-cloud convergence
 118 is associated with moister sub-cloud and cloud-base layers. The converse is true for sub-cloud
 119 divergence. For flight-day averages, the strongest anti-correlation in the vertical occurs at 670 m
 120 ($r=-0.67$). To test whether SMOCS contribute to or are caused by such mesoscale variability,
 121 we investigate time-lag correlations between \mathcal{D}_{sc} and specific humidity (q). The strongest anti-
 122 correlation occurs in the cloud-base layer at 0 h (Fig. 3f), whereas the strongest response of
 123 q_{sc} occurs 2-3 h later. The strengthening of the anti-correlation between \mathcal{D}_{sc} and q_{sc} with time
 124 indicates the direction of causality, i.e. SMOCs amplify sub-cloud moisture variance.

125 Here, we develop a hypothesis of how SMOCs amplify the bottom-heavy moisture fluctua-
 126 tions (see bottom schematic in Fig. 5). In the rising branches, sub-cloud convergence increases
 127 the shallow-convective mass flux into the cloud-base layer [6, 24], which moistens cloud base.
 128 The moistened cloud-base reduces the drying efficiency of entrainment, a term representing
 129 small-scale mixing of dry air at cloud-base into the sub-cloud layer. Albright et al. [25] show
 130 that while entrainment is the dominant term balancing surface fluxes in the sub-cloud mass
 131 budget, the modulation of entrainment drying primarily results from moisture variability above
 132 the sub-cloud layer. Hence, with a moister cloud-base layer, the drying of the sub-cloud layer
 133 by entrainment becomes less efficient, thereby allowing surface moisture fluxes to accumulate

134 moisture in the layer. The argument applies conversely for the descending branch. This process
 135 would lead to an accumulation of moisture in the sub-cloud layer of the ascending branch, and
 136 a corresponding moisture deficit in the descending branch. This bottom heaviness is consistent
 137 with observations (Figs 3c and 3f).

138 Our hypothesis for the bottom-heavy moisture variance comes with two inferences. Firstly,
 139 the process is self limiting, as the moistening of the sub-cloud layer is proportional to its moisture
 140 deficit, which scales with cloud base height, thus potentially setting a limit to how large the
 141 moisture variance could be. Secondly, the time required for surface fluxes to respond to the
 142 change in entrainment drying efficiency means that SMOCs' moistening capacity has a time-
 143 dependence, i.e. the bottom heaviness is not an instantaneous response to SMOCs. This is
 144 consistent with the anti-correlations in Fig. 2b being stronger over flight-day means ($\sim 7-8$ h)
 145 than over circling-set means (~ 3 h).

146 A maintenance of moist and dry branches in circulations will result in horizontal gradients
 147 of buoyancy and radiative cooling. Let's assume the lower and upper quartiles in q' and net
 148 longwave cooling, Q'_{LW} (Fig. 3c & d) represent the spatial differences between ascending and
 149 descending branches. The ascending branch (Q1) shows larger radiative cooling in the sub-
 150 cloud layer, which is opposite to what is expected from a circulation driven by radiative cooling
 151 differences [26]. Differences in shortwave heating between the composites are negligible (not
 152 shown). SMOCs are thus not driven by differential radiative cooling, at least during EUREC⁴A.
 153 One potential driver for circulations though is the buoyancy gradient arising from the moisture
 154 difference [27]. Although the time-lag analysis suggests that buoyancy gradients do not trigger
 155 circulations, they likely amplify or maintain SMOCs. While studies suggest differences in both
 156 radiative cooling [26, 28, 29] and moisture-induced buoyancy [27, 29, 30] as possible causes for
 157 shallow circulations, at the scales observed in our data, it seems like the former inhibits SMOCs
 158 and the latter maintains or amplifies them.

159 A natural question then is how do SMOCs arise. Janssens et al. [12], based on minimal-
 160 physics large eddy simulations (LES), argue that they are triggered by shallow convection's
 161 intrinsic property to create unstable scale-growth in mesoscale moisture fields. Our findings
 162 of SMOCs being ubiquitous also in nature lends strength to their argument that SMOCs are
 163 indeed a signature of an intrinsic instability of the tropical atmosphere. However, in contrast
 164 to the bottom-heavy moisture variance associated with SMOCs in EUREC⁴A data, LES show
 165 largest moisture variance near cloud-top and negligible variance in the sub-cloud layer [10, 11,

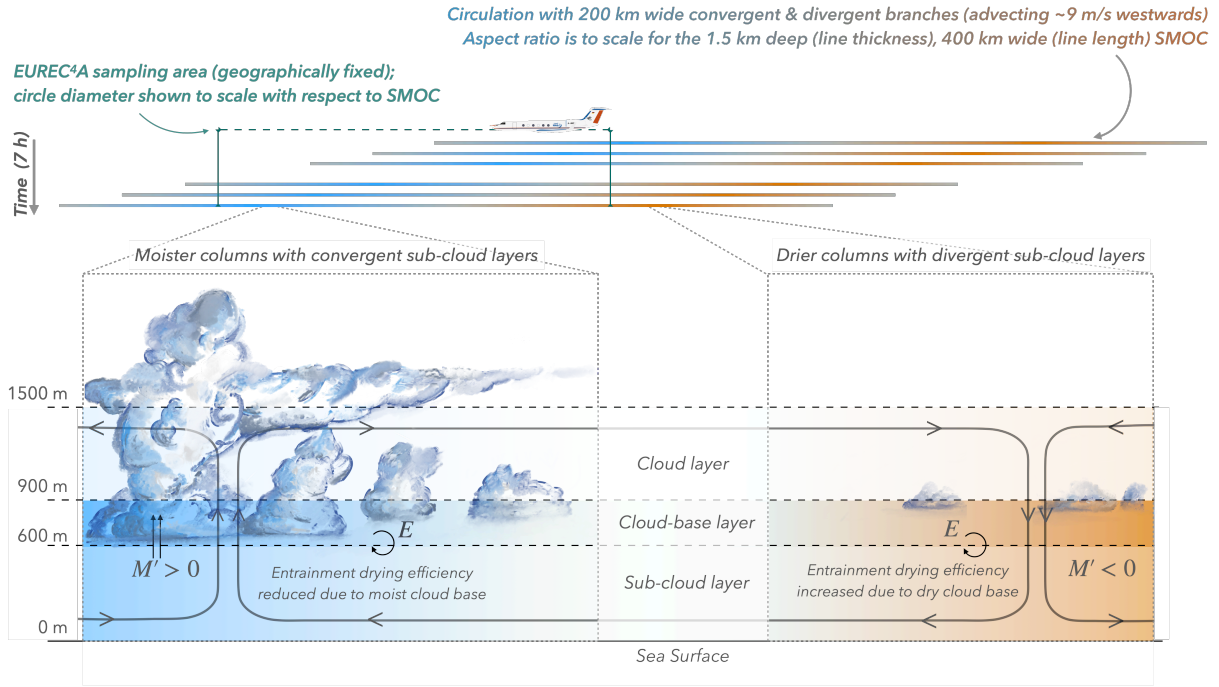


Figure 5: Schematic of our SMOCs hypothesis | E stands for entrainment rate and M' for shallow convective mass flux anomaly. The blue and brown hues represent moisture anomalies. The streamline shows the sense of the envisioned circulation. The aspect ratio of the advected SMOC at the top is shown to scale, underscoring the shallowness of the circulations. For depiction, it is assumed that conditions remain steady during the advection.

166 12]. In LES, the circulation-moisture interplay is shown to form a positive feedback, which
 167 is energized by latent heating anomalies in the cloud layer and their balance by the WTG
 168 adjustment. Although this mechanism explains the top-heavy variance, it is unclear whether
 169 such arguments would also be consistent with the bottom-heavy moisture variance associated
 170 with SMOCs in EUREC⁴A data. While SMOCs may be triggered by condensation-driven heating
 171 anomalies, their strength and associated moisture variance may be modulated by factors such
 172 as precipitation [10, 31, 32], radiative cooling differences [26, 33] and sea-surface temperature
 173 gradients [34].

174 Conclusion

175 EUREC⁴A measurements provide observational evidence for the prevalence of shallow mesoscale
 176 overturning circulations (SMOCs) in the trades and their influence on mesoscale moisture vari-
 177 ance. Specifically:

- 178 • Measurements show an anti-correlation between divergence in the sub-cloud and cloud
 179 layers. We interpret this dipole as being indicative of shallow overturning circulations.

- 180 • The EUREC⁴A measurements allow us to assess that the low-level divergence in ERA5 are
181 representative of the measurements, even if the measurements are not being assimilated.
- 182 • With ERA5, we show that SMOCs are usually elongated features of ~ 100 -200 km and are
183 ubiquitous (covering on average 58% of a $10^\circ \times 10^\circ$ domain), thus explaining the large
184 variability in mesoscale vertical velocity observed in the trades.
- 185 • Sub-cloud convergence is correlated with moister sub-cloud and cloud-base layers, indicat-
186 ing a bottom-heavy moisture variance. By affecting the efficiency of entrainment drying,
187 SMOCs likely amplify moisture variance by extending the moisture fluctuations at cloud
188 base down to the subcloud-layer.
- 189 • Convergent sub-cloud layers are 0.7 g/kg moister and radiate energy at rates that lead to
190 0.3 K/day larger longwave cooling rates than divergent sub-cloud layers, indicating that
191 SMOCs are unlikely to be driven by radiative anomalies.

192 The ubiquity of SMOCS in EUREC⁴A observations and their coupling to mesoscale mois-
193 ture fluctuations [and cloudiness; 5, 6] indicate the mesoscale's control on how clouds couple to
194 climate. The scale of the dominant energy in SMOCs is comparable to the grid scale of current
195 climate models [~ 100 km; 35], and if represented in these models, will likely be aliased to much
196 larger scales. Therefore, exploring the instabilities and competing factors that drive SMOCs
197 and the associated moisture fluctuations will improve our understanding of processes controlling
198 cloud amount and organization. In this regard, differences between models and measurements
199 (such as those in moisture variance) merit further investigation, something aided by our demon-
200 stration of the reanalyses' ability to represent such circulations. Such investigations are further
201 motivated by Vogel et al. [6], who show with EUREC⁴A observations that the variability in
202 mesoscale vertical velocities, which we attribute to SMOCs, substantially controls variability of
203 cloud amount in the trades.

204 Acknowledgments

205 The authors thank everyone who made the organization, collection and processing of EUREC⁴A
206 measurements possible. GG thanks Peter Blossey, Kerry Emanuel and Martin Janssens for in-
207 sightful discussions and Hans Segura for his feedback on the manuscript. SB and RV were funded
208 by the European Research Council EUREC⁴A grant agreement 694768. AKN was funded by

209 the Deutsche Forschungsgemeinschaft (DFG, German Research Foundation) under Germany's
210 Excellence Strategy – EXC 2037 ‘CLICCS - Climate, Climatic Change, and Society’ – Project
211 Number: 390683824. BS acknowledges support from H2020 funding (CONSTRAIN grant no
212 820829). HALO's operations during EUREC⁴A were funded by the Max Planck Society (MPG),
213 the German Research Foundation (DFG), the German Meteorological Weather Service (DWD)
214 and the German Aerospace Center (DLR).

215 Code and Data Availability

216 The EUREC⁴A circle measurements we used are from the JOANNE dataset v2.0.0 [16] and can
217 be accessed with the DOI 10.25326/246. The radiative cooling profiles are from the dataset
218 made available by Albright et al. [36] with the DOI 10.25326/78. The ERA5 data was accessed
219 from Copernicus Climate Change Service (C3S) Climate Data Store (CDS) [37]. The data for
220 the data-denial experiments performed with the IFS model used in this study are available
221 with the following DOIs: ‘ctrl’ at 10.21957/4vgx-3f28 ; ‘nd’ at 10.21957/zfxz-3h02 and ‘ndnr’
222 at 10.21957/7zx9-6084 [38]. The code to make the plots in this manuscript and to perform the
223 relevant analyses will be made available with a DOI.

224 References

- 225 [1] Sandrine Bony et al. “Clouds, circulation and climate sensitivity”. In: *Nature Geoscience*
226 8.4 (Mar. 2015), pp. 261–268.
- 227 [2] Louise Nuijens and A Pier Siebesma. “Boundary layer clouds and convection over subtrop-
228 ical oceans in our current and in a warmer climate”. In: *Current Climate Change Reports*
229 5.2 (2019), pp. 80–94.
- 230 [3] Gerald A. Meehl et al. “Context for interpreting equilibrium climate sensitivity and tran-
231 sient climate response from the CMIP6 Earth system models”. In: *Science Advances* 6.26
232 (2020), eaba1981.
- 233 [4] Mark D. Zelinka et al. “Causes of higher climate sensitivity in CMIP6 models”. In: *Geo-*
234 *physical Research Letters* (Jan. 2020).

- 235 [5] Geet George, Bjorn Stevens, Sandrine Bony, Marcus Klingebiel, and Raphaela Vogel. “Ob-
236 served impact of meso-scale vertical motion on cloudiness”. In: *Journal of the Atmospheric*
237 *Sciences* (2021).
- 238 [6] Raphaela Vogel et al. *Strong cloud-circulation coupling explains weak trade cumulus feed-*
239 *back*. under review in *Nature*. 2022.
- 240 [7] Matthew D Lebsock, Tristan S L’Ecuyer, and Robert Pincus. “An observational view
241 of relationships between moisture aggregation, cloud, and radiative heating profiles”. In:
242 *Shallow Clouds, Water Vapor, Circulation, and Climate Sensitivity*. Springer, 2017, pp. 65–
243 82.
- 244 [8] Paulo Ceppi et al. “Cloud feedback mechanisms and their representation in global climate
245 models”. In: *Wiley Interdisciplinary Reviews: Climate Change* 8.4 (2017), e465.
- 246 [9] BE Mapes. “Gregarious convection and radiative feedbacks in idealized worlds”. In: *Jour-*
247 *nal of Advances in Modeling Earth Systems* 8.2 (2016), pp. 1029–1033.
- 248 [10] Christopher S. Bretherton and Peter N. Blossey. “Understanding Mesoscale Aggregation
249 of Shallow Cumulus Convection Using Large-Eddy Simulation”. In: *Journal of Advances*
250 *in Modeling Earth Systems* 9.8 (2017), pp. 2798–2821.
- 251 [11] Pornampai Narenpitak et al. “From Sugar to Flowers: A Transition of Shallow Cumulus
252 Organization During ATOMIC”. In: *Journal of Advances in Modeling Earth Systems* 13.10
253 (2021).
- 254 [12] M. Janssens et al. “Non-precipitating shallow cumulus convection is intrinsically unstable
255 to length-scale growth”. In: *Journal of the Atmospheric Sciences* (under review).
- 256 [13] Sandrine Bony et al. “EUREC4A: A field campaign to elucidate the couplings between
257 clouds, convection and circulation”. In: *Surveys in Geophysics* (Sept. 2017), pp. 1–40.
- 258 [14] B. Stevens et al. “EUREC⁴A”. In: *Earth System Science Data* 13.8 (2021), pp. 4067–4119.
- 259 [15] H. Konow et al. “EUREC⁴A’s HALO”. In: *Earth System Science Data* 13.12 (2021),
260 pp. 5545–5563.
- 261 [16] G. George et al. “JOANNE: Joint dropsonde Observations of the Atmosphere in tropical
262 North atlAntic meso-scale Environments”. In: *Earth System Science Data* 13.11 (2021),
263 pp. 5253–5272.

- 264 [17] Minghua Zhang et al. “The CGILS experimental design to investigate low cloud feedbacks
265 in general circulation models by using single-column and large-eddy simulation models”.
266 In: *Journal of Advances in Modeling Earth Systems* 4.4 (Apr. 2012).
- 267 [18] Adam H. Sobel, Johan Nilsson, and Lorenzo M. Polvani. “The Weak Temperature Gradient
268 Approximation and Balanced Tropical Moisture Waves”. In: *Journal of the Atmospheric
269 Sciences* 58.23 (2001), pp. 3650–3665.
- 270 [19] Dennis L. Hartmann and Kristin Larson. “An important constraint on tropical cloud -
271 climate feedback”. In: *Geophysical Research Letters* 29.20 (2002), pp. 12-1-12-4.
- 272 [20] Sally A. McFarlane, James H. Mather, and Thomas P. Ackerman. “Analysis of tropi-
273 cal radiative heating profiles: A comparison of models and observations”. In: *Journal of
274 Geophysical Research: Atmospheres* 112.D14 (2007).
- 275 [21] Hans Hersbach et al. “The ERA5 global reanalysis”. In: *Quarterly Journal of the Royal
276 Meteorological Society* (June 2020).
- 277 [22] S. Bony et al. “On dynamic and thermodynamic components of cloud changes”. In: *Climate
278 dynamics* 22.2-3 (Mar. 2004), pp. 71–86.
- 279 [23] Timothy A. Myers and Joel R. Norris. “Observational evidence that enhanced subsidence
280 reduces subtropical marine boundary layer cloudiness”. In: *Journal of climate* 26.19 (Oct.
281 2013), pp. 7507–7524.
- 282 [24] Raphaela Vogel, Sandrine Bony, and Bjorn Stevens. “Estimating the Shallow Convec-
283 tive Mass Flux from the Subcloud-Layer Mass Budget”. In: *Journal of the Atmospheric
284 Sciences* 77.5 (May 2020), pp. 1559–1574.
- 285 [25] Anna Lea Albright et al. “A new conceptual picture of the trade-wind transition layer”.
286 In: *Journal of the Atmospheric Sciences* (submitted).
- 287 [26] Ann Kristin Naumann, Bjorn Stevens, and Cathy Hohenegger. “A moist conceptual model
288 for the boundary layer structure and radiatively driven shallow circulations in the trades”.
289 In: *Journal of the Atmospheric Sciences* 76.5 (May 2019), pp. 1289–1306.
- 290 [27] Da Yang. “Boundary Layer Height and Buoyancy Determine the Horizontal Scale of Con-
291 vective Self-Aggregation”. In: *Journal of the Atmospheric Sciences* 75.2 (2018), pp. 469–
292 478.

- 293 [28] Caroline Muller and Sandrine Bony. “What favors convective aggregation and why?” In:
294 *Geophysical Research Letters* 42.13 (2015), pp. 5626–5634.
- 295 [29] Caroline Muller et al. “Spontaneous Aggregation of Convective Storms”. In: *Annual Review*
296 *of Fluid Mechanics* 54.1 (2022), pp. 133–157.
- 297 [30] Da Yang. “A shallow-water model for convective self-aggregation”. In: *Journal of the*
298 *Atmospheric Sciences* 78.2 (2021), pp. 571–582.
- 299 [31] A. Seifert and T. Heus. “Large-eddy simulation of organized precipitating trade wind
300 cumulus clouds”. In: *Atmospheric Chemistry and Physics* 13.11 (2013), pp. 5631–5645.
- 301 [32] T. J. Anurose et al. “Understanding the Moisture Variance in Precipitating Shallow
302 Cumulus Convection”. In: *Journal of Geophysical Research: Atmospheres* 125.1 (2020).
303 e2019JD031178 10.1029/2019JD031178, e2019JD031178.
- 304 [33] Allison A. Wing and Kerry A. Emanuel. “Physical mechanisms controlling self-aggregation
305 of convection in idealized numerical modeling simulations”. In: *Journal of Advances in*
306 *Modeling Earth Systems* 6.1 (2014), pp. 59–74.
- 307 [34] A. Foussard, G. Lapeyre, and R. Plougonven. “Response of Surface Wind Divergence to
308 Mesoscale SST Anomalies under Different Wind Conditions”. In: *Journal of the Atmo-*
309 *spheric Sciences* 76.7 (2019), pp. 2065–2082.
- 310 [35] V. Balaji et al. “Requirements for a global data infrastructure in support of CMIP6”. In:
311 *Geoscientific Model Development* 11.9 (2018), pp. 3659–3680.
- 312 [36] A. L. Albright et al. “Atmospheric radiative profiles during EUREC⁴A”. In: *Earth System*
313 *Science Data* 13.2 (2021), pp. 617–630.
- 314 [37] H Hersbach et al. “ERA5 hourly data on single levels from 1979 to present”. In: *Copernicus*
315 *Climate Change Service (C3S) Climate Data Store (CDS)* 10 (2018).
- 316 [38] A. C. M. Savazzi et al. “The representation of winds in the lower troposphere in ECMWF
317 forecasts and reanalyses during the EUREC4A field campaign”. In: *Atmospheric Chemistry*
318 *and Physics Discussions* 2022 (2022), pp. 1–29.
- 319 [39] Sandrine Bony and Bjorn Stevens. “Measuring Area-Averaged Vertical Motions with Drop-
320 sondes”. In: *Journal of the Atmospheric Sciences* 76.3 (Mar. 2019), pp. 767–783.
- 321 [40] Anna Lea Albright et al. “Observed subcloud layer moisture and heat budgets in the
322 trades”. In: *Journal of the Atmospheric Sciences* (2022).

- 323 [41] Geet George. “Observations of meso-scale cloudiness and its relationship with cloudiness in
 324 the tropics”. PhD thesis. Staats-und Universitätsbibliothek Hamburg Carl von Ossietzky,
 325 2021.
- 326 [42] Irina Sandu et al. *On the causes of systematic forecast biases in near-surface wind direction
 327 over the oceans*. Tech. rep. ECMWF Technical Memorandum, 2020.
- 328 [43] Christopher Lloyd. *Spatial data analysis: an introduction for GIS users*. Oxford university
 329 press, 2010.
- 330 [44] Stéfan van der Walt et al. “scikit-image: image processing in Python”. In: *PeerJ* 2 (June
 331 2014), e453.

332 Methods

333 EUREC⁴A Dropsonde Measurements

334 The field campaign EUREC⁴A took place in January-February, 2020 over the tropical north-
 335 Atlantic upwind of Barbados [see campaign overview in 14]. A core observation of EUREC⁴A was
 336 area-averaged horizontal mass divergence and vertical velocity profiles derived from dropsonde
 337 measurements along the circumference of a circular flight path [39]. In EUREC⁴A, the circular
 338 flight path was fixed to facilitate statistical sampling, with the centre at 57.67°W, 13.31°N and
 339 a diameter of 222.82 km (hereafter called EUREC⁴A circles), and flown by the German High
 340 Altitude and Long range (HALO) aircraft. To keep the sampling consistent, here we exclude
 341 HALO’s first (19.01.2020) and final (15.02.2020) research flights of the campaign and use data
 342 from 65 circles flown over the remaining 11 research flights, with a typical flight including
 343 6 circles. Each circle typically launched 12 dropsondes spaced equally along the circumference
 344 over a period of an hour. On most flight days, HALO flew two sets of three circles each, called
 345 *circling sets*, with an excursion in between aimed at sampling upwind conditions. The two
 346 circling sets of a flight were carried out over a period of 7-8 hours; here termed as a *flight-day*.
 347 An overview of the circles flown during EUREC⁴A and the dropsondes therein is provided in
 348 George et al. [16].

349 The dataset *Joint dropsonde Observations of the Atmosphere in tropical North atlaNtic*
 350 *mesoscale Environments*, with the backronym JOANNE [16], provides measurements from the
 351 EUREC⁴A dropsondes. We use Level-4 data of JOANNE which provides the area-averaged
 352 quantities at 10 m vertical spacing from the circle measurements, such as horizontal mass diver-

353 gence (\mathcal{D}) and specific humidity (q). The measured quantities are from the surface up to 9.5 km,
 354 which was the typical flight altitude during the circles. From the dataset provided by Albright
 355 et al. [36], we use the net radiative cooling rates, with circle values obtained by averaging over
 356 sondes in the circle.

357 Throughout the study, we use the terms *sub-cloud layer*, *cloud-base layer* and *cloud layer*
 358 (referred to as ‘sc’, ‘cb’ and ‘c’ subscripts) to indicate altitude intervals of 0-600 m, 600-900 m
 359 and 900-1500 m from the surface, respectively (also indicated in Fig. 1c). We define the cloud-
 360 base layer as an extended transition layer between the sub-cloud and cloud layers to account for
 361 thermodynamic variability that is most tightly coupled to that within the sub-cloud layer [40].
 362 We explored, but found little benefit of trying to adapt these altitude intervals based on the
 363 specific structure of the trade-wind layer for any given day [also see 41]. The symbol ‘ \prime ’ is also
 364 used to indicate the anomaly from campaign mean. For example, \mathcal{D}'_{sc} is the divergence anomaly
 365 from time-mean, averaged over the sub-cloud layer.

366 **ERA5 divergence and comparison with EUREC⁴A**

367 We use \mathcal{D} from ERA5 reanalysis products for time-period between 20-01-2020 00:00 UTC and
 368 21-02-2020 00:00 UTC (parameter ID 155) available at 0.25° and 1 h intervals. First, we check
 369 the reliability of ERA5 divergence, by comparing it with the circle observations. To make
 370 a comparison collocated in space-time, we average ERA5 divergence spatially over grid-boxes
 371 included within the standard-circle area for the hourly time-step nearest to the mean time of each
 372 circle from observations. Figure ED.1 shows the agreement between these divergence profiles
 373 from ERA5 and the corresponding ones from JOANNE averaged for every flight-day. Whereas
 374 the profiles shown are averages over the flight-day, the estimate of r-values in the figure are from
 375 values from all individual profiles in that day. Thus, the reanalysis’ agreement of divergence with
 376 observations is also at the circle time-scale (1 h) and not just when averaged over the flight-day
 377 (6-7 h). The vertical structure of divergence simulated by ERA5 is the same as that seen in the
 378 circle observations for most days, thus lending confidence in the use of reanalysis fields to study
 379 the spatial and temporal variability in divergence.

380 The ERA5 products have assimilated information from the EUREC⁴A dropsondes and ra-
 381 diosondes. To check the influence of assimilation, we check the difference in divergence simulated
 382 by data-denial experiments. These experiments are the same as those described by Savazzi et al.
 383 [38], where a control simulation (‘ctrl’) similar to the ERA5 operational product is run along

384 with two data-denial experiments – one with no EUREC⁴A dropsondes (‘nd’) and the other
 385 with no EUREC⁴A dropsondes and radiosondes (‘ndr’) assimilated. We compare profiles be-
 386 tween JOANNE and the experiments when the timestamps are within an hour of each other.
 387 The experiments have outputs available at 6 h intervals, and therefore, we only have 15 instances
 388 when \mathcal{D} can be compared with JOANNE. Fig. ED.2 shows the square root of the mean squared
 389 error between \mathcal{D} in the three experiments and \mathcal{D} in JOANNE (RMSE $_{\mathcal{D}}$). The assimilation re-
 390 sults in very little improvement in the simulated fields of divergence. A similar conclusion was
 391 drawn by Savazzi et al. [38] for horizontal wind in the lowest 2 km. We believe that assimi-
 392 lation of near-surface horizontal winds from satellite-based scatterometers constrains the ERA5
 393 near-surface divergence over ocean, making it possible to get an accurate vertical structure of
 394 \mathcal{D} . The small impact of the soundings’ assimilation of soundings is explained more generally by
 395 Sandu et al. [42] as “what often happens when one observing system is withdrawn from the data
 396 assimilation system is that other observing systems compensate for its loss and play a bigger
 397 role in constraining the analysis.”

398 Segmenting SMOC objects

399 To detect SMOC objects in the ERA5 \mathcal{D}_{sc} field, we introduce a crude measure to detect which
 400 gridboxes can be included as being part of SMOCs objects. All gridboxes which have opposite
 401 signs of \mathcal{D}'_{sc} and \mathcal{D}'_c are considered SMOC cells (see Fig. 4a and Fig. ED.3). Such cells are
 402 further classified as either convergent cells if $\mathcal{D}'_{sc} < 0$ or divergent if $\mathcal{D}'_{sc} > 0$. Furthermore,
 403 the domain is segmented into multiple clusters of convergent and divergent cells based on a
 404 neighbor-identifying scheme where up to two orthogonal hops are made to consider a gridbox
 405 as a neighbor, or what is also known as a Queen’s contiguity case in spatial autocorrelation
 406 analysis [43] (see Fig. 4b). We use the `label` function from the `measure` module of Python’s
 407 `scikit-image` package (v0.19.2) [44] to perform this.

408 To get an estimation of the horizontal scale of these clusters, we estimate their major and
 409 minor axes, if they were fitted to an ellipse. Thus, the major and minor axes are defined as
 410 the larger and smaller second moments of area of these clusters, respectively. The first moment
 411 of area provides the coordinates for the centroids of clusters shown in Fig. 4b. The effective
 412 diameter (d_{eff}) of the clusters is the diameter of a circle equivalent in area to the area of the
 413 cluster. To avoid irregularities due to the coarse-resolution of the ERA5 domain, we only consider
 414 clusters with major axis length greater than 0.75° as SMOC objects.

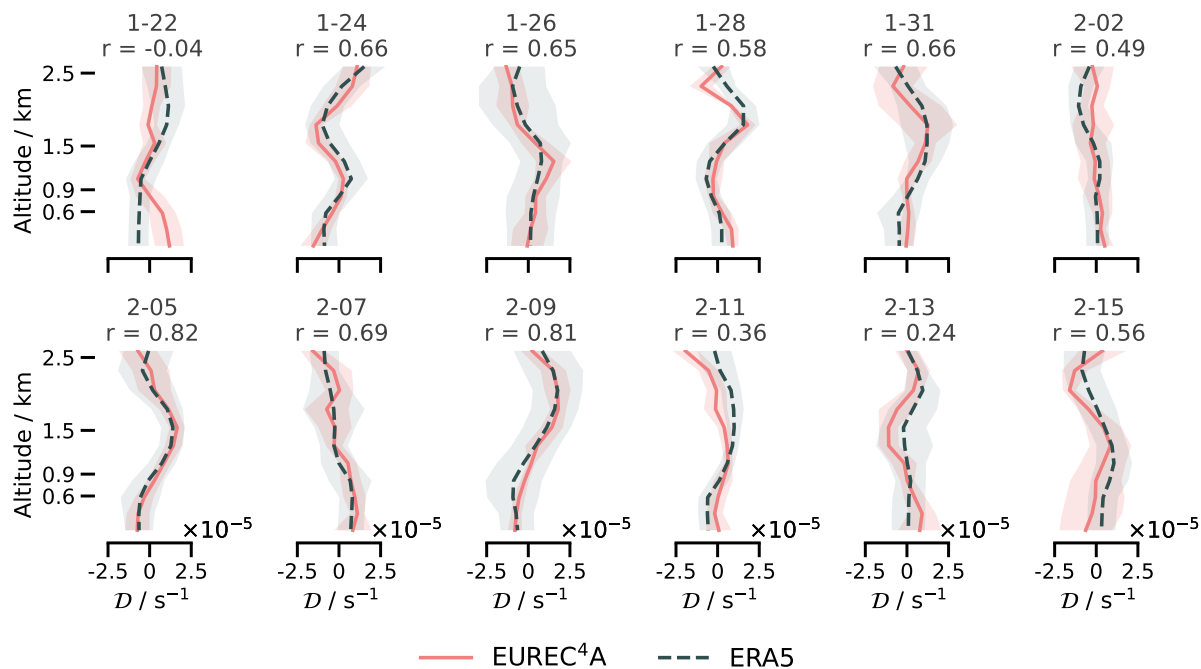
415 **Extended Data**

Figure ED.1: Profiles of flight-day mean divergence from EUREC⁴A dropsonde measurements (JOANNE; red solid line) shown with the interquartile range (red shaded). Corresponding profiles from ERA5 by averaging over gridboxes within the circle, with time-steps nearest to the ones included in the JOANNE flight-day mean (grey dotted line) and the interquartile range (grey shaded) therein are overlaid. Above each profile, the flight date is given along with the correlation r -value between JOANNE and ERA5 profiles for all circles on that flight-day.

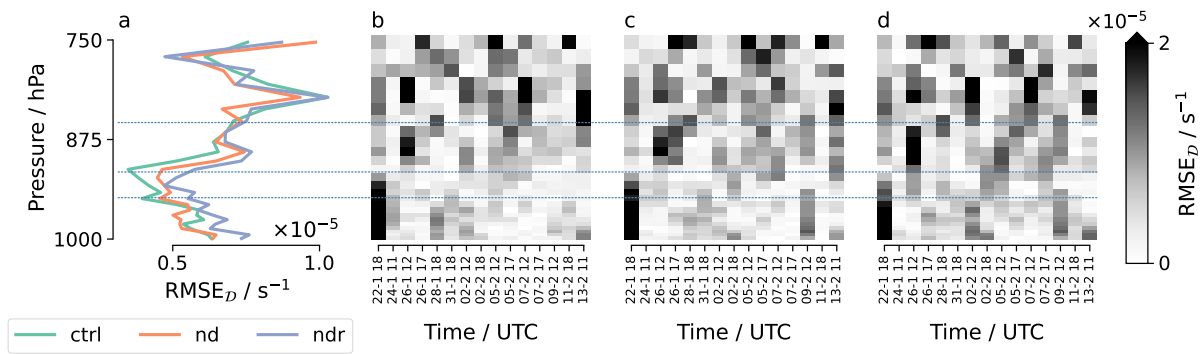


Figure ED.2: (a) Vertical profiles of $\text{RMSE}_{\mathcal{D}}$ for the control and two data-denial experiments. Hues show $\text{RMSE}_{\mathcal{D}}$ for experiments (b) ‘ctrl’, (c) ‘nd’ and (d) ‘ndnr’ at all instances where times-tamps in the experiments are within an hour of available circle measurements from JOANNE. The tick labels on the X-axis are in the format ‘DD-M H’, where D, M and H stand for date, month and hour, respectively. The overlaid horizontal lines (dotted blue) indicate, from top to bottom, the tops of the sub-cloud layer, cloud-base layer and cloud layer.

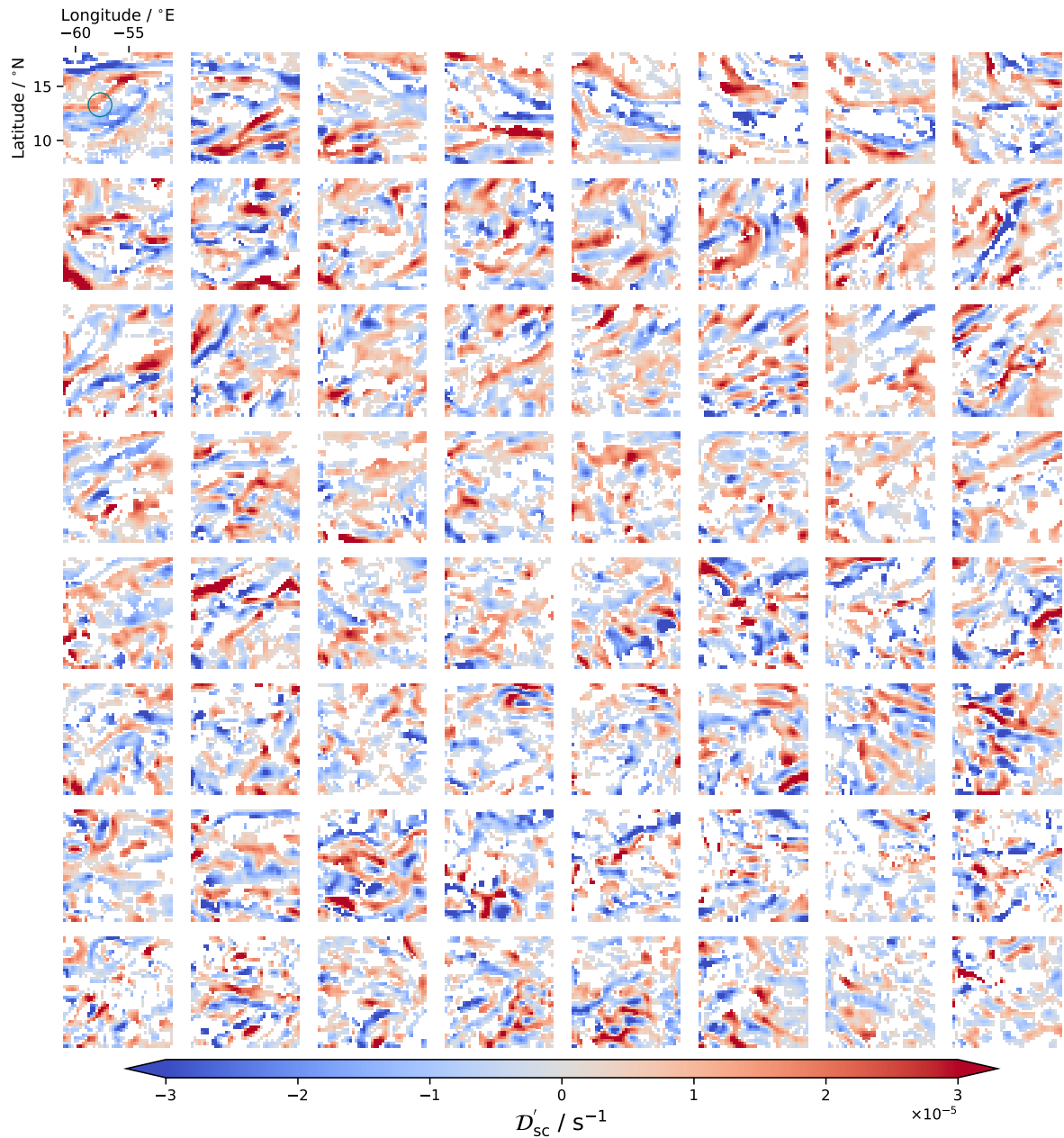


Figure ED.3: Spatio-temporal ubiquity of SMOCs in the trades shown by ERA5 D'_{sc} plotted over a $10^\circ \times 10^\circ$ domain for the EUREC⁴A period at every 12 h timestep. Only gridboxes which have opposite signs of divergence anomaly in the sub-cloud and cloud layer are shaded, reds showing converging airmasses in the sub-cloud layer and blue diverging. Unshaded gridboxes (in white) are where sub-cloud and cloud layers have same sign of D' . The first box shows the spatial scale of the domain along with a circle (teal) showing scale of EUREC⁴A measurements.